



HAL
open science

A passive optical fiber sensor based on Fabry-Perot interferometry for bipolar electrostatic monitoring of insulating dielectrics

Jiawei Zhang, Zifan Ye, Li Wang, Zelei Zhang, Fan Xu, Weichen Dang, Takao Matsumoto, Sombel Diahm, Chatchai Putson

► To cite this version:

Jiawei Zhang, Zifan Ye, Li Wang, Zelei Zhang, Fan Xu, et al.. A passive optical fiber sensor based on Fabry-Perot interferometry for bipolar electrostatic monitoring of insulating dielectrics. *High Voltage*, 2023, 8 (4), pp.682-689. 10.1049/hve2.12339 . hal-04778078

HAL Id: hal-04778078

<https://ut3-toulouseinp.hal.science/hal-04778078v1>

Submitted on 5 Dec 2024

HAL is a multi-disciplinary open access archive for the deposit and dissemination of scientific research documents, whether they are published or not. The documents may come from teaching and research institutions in France or abroad, or from public or private research centers.


L'archive ouverte pluridisciplinaire **HAL**, est destinée au dépôt et à la diffusion de documents scientifiques de niveau recherche, publiés ou non, émanant des établissements d'enseignement et de recherche français ou étrangers, des laboratoires publics ou privés.



Distributed under a Creative Commons Attribution 4.0 International License

ORIGINAL RESEARCH

A passive optical fiber sensor based on Fabry-Perot interferometry for bipolar electrostatic monitoring of insulating dielectrics

Jiawei Zhang¹  Zifan Ye¹ | Li Wang¹ | Zelei Zhang¹ | Fan Xu¹ | Weichen Dang¹
Takao Matsumoto¹ | Sombel Diaham² | Chatchai Putson³

¹ School of Electrical Engineering, Xi'an University of Technology, Xi'an, Shaanxi, China

² Université de Toulouse, UPS, INPT, LAPLACE (Laboratoire Plasma et Conversion d'Energie), F-31062 Toulouse cedex 9, France

³ Materials Physics Laboratory, Department of Physics, Faculty of Science, Prince of Songkla University (PSU), Songkhla 90112, Thailand

Correspondence

Jiawei Zhang, School of Electrical Engineering,
Xi'an University of Technology, Xi'an, Shaanxi
710048, China.
Email: jwzhang@xaut.edu.cn

Associate Editor:

Guoming Ma

Funding information

National Natural Science Foundation of China,
Number: 62061136009, 51877031.

Abstract

The measurement of the surface charge on the insulating dielectrics is critical to estimate the insulation strength of electrical equipment in operation. Unavoidable interactions with the electromagnetic field, however, generally result in distortion measurement of active sensor. Thus, it is of great significance to investigate a passive sensor for monitoring the deposited charge. Here, a passive optical fiber electrostatic sensor is developed on the principle of Fabry-Perot (F-P) interference to quantify the surface potential of the insulating dielectrics. The sensitivity of quantifying the electrostatic charge is explored in terms of the wavelength shift in interference spectrum and the linear correlation is 0.99. Meanwhile, the sensor can identify a negative quadratic trend with the increase of the surface roughness of the insulating dielectrics. The merits of the proposed sensor such as passive monitoring, bipolar electrostatic detection and the excellent ability of anti-electromagnetic interference are highlighted in the results. Hence, this sensor can serve as an effective tool to monitor the electrostatic charge in the fields of smart electrical equipment, fuel transportation, aerospace, integrate circuit (IC), etc.

1 INTRODUCTION

Preventing electrostatic discharge is nowadays of important pathway in performance preservation, lifetime extension, and safety risk reduction of devices in the fields of smart grid[1], fuel transportation[2], aerospace[3], integrated circuit (IC)[4]. For instance, the decrease of withstand voltage of the spacer in the gas-insulated transmission lines (GIL) will be induced by the electrostatic charge accumulation[1,5], resulting in threats to the smart power grid. Again, failure of the radio system of aircraft and the reliability decline of

semiconductor devices will be caused by the electrostatic discharge[6,7]. Thus, it is urgently desired to monitor the electrostatic discharge in a diverse range of engineering applications. Currently, three methods can be used to measure the surface charge including the dust figure technique[8], electrostatic probe (EP)[5,9-10], and the optical Pockels technique[5,11].

Dust figure technique is the earliest method to measure the surface charge. It could easily identify the polarity and distribution of the surface charge, rather than obtaining the value of the surface potential quantitatively. The EP method proposed by D. K. Davies[9] in 1967 can be used to measure the surface charge of the electrical equipment

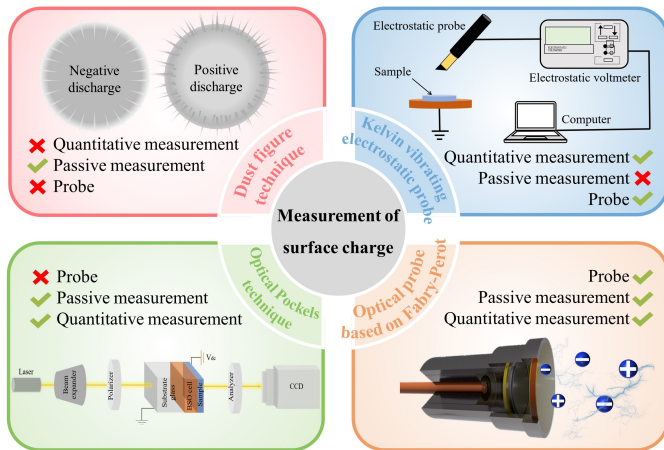


Fig. 1 Diagram of the measurement methods of surface charge

quantitatively[12]. In a follow-up study, the use of an active Kelvin vibrating probe improved the accuracy of the measurements, but the advantage of passive measurement was lost[10]. Then, the passive method for measuring the surface charge based on the optical Pockels technology has been extensively researched in recent years. The electro-optical crystals with Pockels effect such as lithium niobate (LiNbO_3) have been used to evaluate the deposited surface charge quantitatively. This optical Pockels technology can be realized by expanded He-Ne laser, the optical elements of the polarizer, analyzer, et al[13]. Although the optical Pockels technique has the advantage of passive measurement, it is difficult to assemble a probe due to the miscellaneous optical elements, which limits its commercial application.

In recent years, extensive studies have been conducted on the optical fiber sensors based on the principle of Fabry-Perot (F-P) interference in the partial discharge detection of the transformer due to their merits of high sensitivity, high accuracy, high signal-to-noise ratio[14-20], etc. Meanwhile, the development of advanced functional materials enables the development of the sensor for higher-performance[21]. As shown in Fig. 1, an optical fiber electrostatic sensor based on the principle of F-P interference is developed and fabricated in order to overcome the limitations of the Kelvin vibrating probe and the optical Pockels technology. In this paper, an optical F-P electrostatic sensor was proposed to measure the surface potential of polyimide (PI) in the electrical equipment[22] after

the corona discharge and detect the polarities of six insulating objects after friction. Meanwhile, the interactive influence between the charge accumulation and the surface morphology was analyzed. These results demonstrate that the surface potential can be monitored in real-time by using the F-P electrostatic sensor proposed in this work which exhibits some merits such as passive monitoring and excellent anti-electromagnetic interference ability. This paper aims to shed light on monitoring the surface potential based on the optical technique and offers the valuable reference for exploring the accumulation characteristic of the surface charge under various roughness of the discharged sample.

2. the Principle and Fabrication of Sensor

2.1. Structural design and fabrication

The F-P electrostatic sensor principally consists of a single-mode fiber (SMF), an electromechanical transducer, and a charge collector, as shown in Fig. 2. The electromechanical transducer is assembled in the sensitive end, and the polished surface of the metal electrodes are regarded as the reflecting surface of the F-P cavity. One end face of the SMF is used as another reflection surface. The F-P cavity consists of aligning the reflection surface of the SMF and the electromechanical transducer. The extrinsic F-P interferometer is used as a sensing cavity to measure imperceptible variation of electrostatic charge. In this structure, the optical coupling between the interference fringes and the cavity length L is obtained by adjusting L to about $500 \mu\text{m}$. The interference spectrum of the F-P cavity in the sensor is shown in Fig. 3(a). The maximum and minimum values correspond to the bright fringe and the dark fringe, respectively. The free spectral range (FSR) of the spectrum is 2.154 nm . Additionally, the length of the cavity can be verified according to Equation (1)[23].

$$L = \frac{\lambda_1 \lambda_2}{2n(\lambda_2 - \lambda_1)} \quad (1)$$

where λ_1, λ_2 are the two wavelengths of adjacent peaks, $n=1$ is the refractive index of the air in the F-P cavity, $\lambda_2 - \lambda_1$ is FSR. The spectral shift will occur when an external signal causes the change in the length of the cavity, as shown in Fig. 3(b). The $\Delta\lambda$ is the spectral shift corresponding to the n th bright fringe when the change occurs in the length of the cavity.

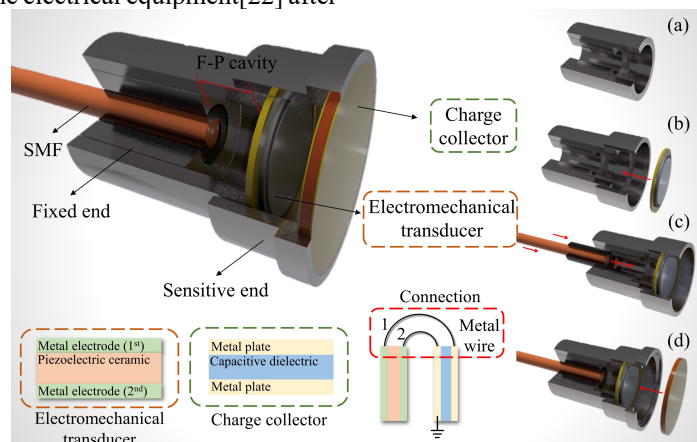


Fig. 2 Structure diagram of the F-P electrostatic sensor

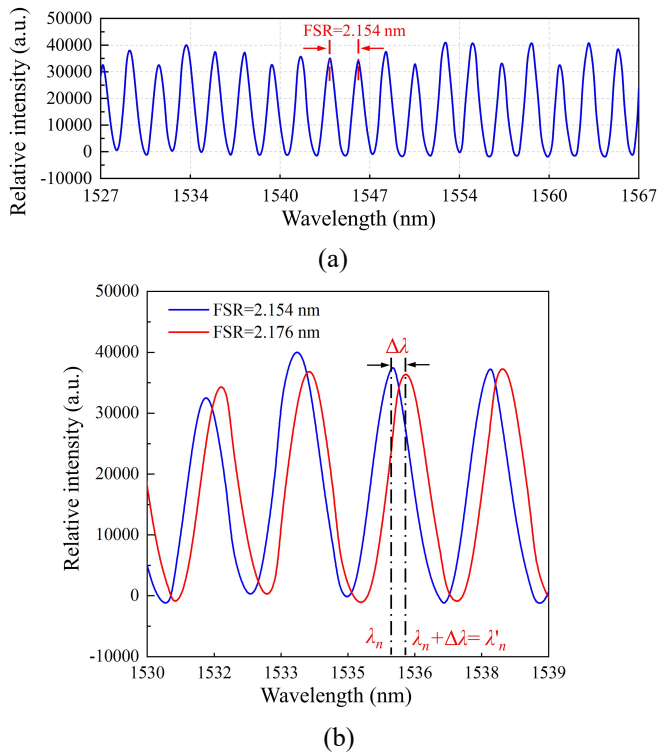


Fig. 3 Interference spectrum of the F-P electrostatic sensor

(a)The interference fringes of the sensor, (b)The spectral shift when the change occurs in the length of the cavity

The fabrication process of the F-P electrostatic sensor is shown as follows.

(a)A stainless mold with an inner/outer diameter of 2.7/20 mm was fabricated to form a F-P cavity structure, whose upper and lower ends constituted to the sensitive end and fixed end, respectively.

(b)The electromechanical transducer was assembled at the sensitive end for high-speed bonding using a cyanoacrylate adhesive. In addition, the functional materials acting as the electromechanical transducer with sandwich structure was composed of a piezoelectric ceramic and polished metal electrodes, as shown in Fig. 2.

(c)The SMF was inserted into the stainless mold from the fixed end and then fixed with a cyanoacrylate adhesive. Notably, the polished surface of the electromechanical transducer was strictly parallel to the SMF.

(d)The charge collector[24] was assembled with the electromechanical transducer by the metal wire to capture the electrostatic charge. Additionally, the charge collector was composed of the capacitive dielectric and metal plates, which formed sandwich structure, as shown in Fig. 2. The sensor was placed for 24 hours to release the viscous stress from the adhesive. It is worth noting that the above processes were performed on the optical platform and the length of the structure was kept at 40 mm.

2.2. Principle of the sensor

The change of the F-P cavity length corresponding to the strain of electromechanical transducer is influenced by the

external electrostatic charge, which is captured by the charge collector.

The piezoelectric equation of the electromechanical transducer is:

$$\varepsilon = d_{33}E \Rightarrow \frac{\Delta L}{d} = d_{33} \frac{U}{d'} \quad (2)$$

Where ε and d are the strain and the axial thickness of the electromechanical transducer, respectively. E and d' are the electric field intensity and the distance in the direction of electric field, respectively. Due to the strain induced by the electrostatic voltage U , the change occurs in the length of the cavity L . In addition, since the change direction of the electric field is the same as the direction of the strain. Therefore, $d=d'$ in Equation (2) and the change in the cavity length ΔL could be written as

$$\Delta L = d_{33}U \quad (3)$$

Where $U=Q/C$, d_{33} is the inverse piezoelectric coefficient of electromechanical transducer, Q is the collected charge, C is the capacitance value of charge collector composed of two parallel metal plates and the dielectric between them. Hence, the charge quantity of the charged object may change with the voltage U across the metal plates of the charge collector due to the electrostatic induction and the charge transfer[25]. In addition, if the piezoelectric ceramic has the giant d_{33} coefficient, a larger ΔL will occur.

In the demodulation process of ΔL , bimodal measurement is to demodulate the cavity length by two adjacent peaks in the interference spectrum. It is assumed that the cavity length before and after the change are L_1 and L_2 , respectively. The definition of two adjacent peaks are n (the corresponding wavelengths are λ_n and λ'_n , respectively) and $n+1$ (the corresponding wavelengths are λ_{n+1} and λ'_{n+1} , respectively). In addition, $\lambda_n + \Delta\lambda = \lambda'_n$, as shown in Fig.3. The peak of the wavelength satisfies the following equations:

$$\frac{4\pi}{\lambda_n} L = 2\pi n, n = 1, 2, 3, \dots \quad (4)$$

$$\frac{4\pi}{\lambda_{n+1}} L = 2\pi(n+1), n = 1, 2, 3, \dots \quad (5)$$

Thus, from Equations (4) and (5), L_1 could be written as

$$L_1 = \frac{\lambda_n \lambda_{n+1}}{2(\lambda_n - \lambda_{n+1})} \quad (6)$$

Similarly, after the cavity length is changed, L_2 could be written as

$$L_2 = \frac{\lambda'_n \lambda'_{n+1}}{2(\lambda'_n - \lambda'_{n+1})} \quad (7)$$

Finally, from Equations (6) and (7), ΔL could be written as:

$$\Delta L = |L_1 - L_2| \quad (8)$$

Therefore, the strain of the electromechanical transducer leads to the change of the cavity length, which further leads to

a modulation of the wavelength of the sensor.

The operating principle of the F-P electrostatic sensor is shown in Fig. 4. The light source is launched via an amplified spontaneous emission (ASE) broadband source (1527~1567 nm) and the ASE has an emission wavelength range covering the C-band. The light emitted by the ASE is transmitted into a 3 dB coupler and then transmitted to the sensor through the optical fiber[26]. Subsequently, the light is reflected on the polished surface of the electromechanical transducer by the end face of SMF, which could form the optical interference, and the interference light is transmitted to the demodulator through 3 dB coupler. When the external electrostatic charge is detected by the F-P electrostatic sensor, the change occurs in the F-P cavity length due to the inverse piezoelectric effect of the electromechanical transducer. Then the wavelength of interference spectrum changes accordingly, which is detected through the demodulator to obtain the signal from external electrostatic charge.

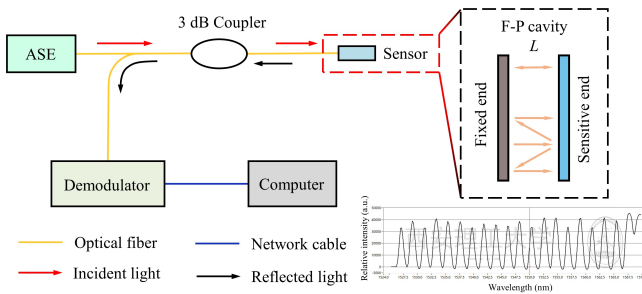


Fig. 4. Schematic diagram of the optical system based on the F-P electrostatic sensor

3. Characteristic of the Sensor

3.1. Response of the sensor

To prove the identification capability of the F-P electrostatic sensor, different samples were tested at a fixed distance, with the relative humidity and temperature kept at 35%~50% and 25 °C, respectively, as shown in Fig. 5.

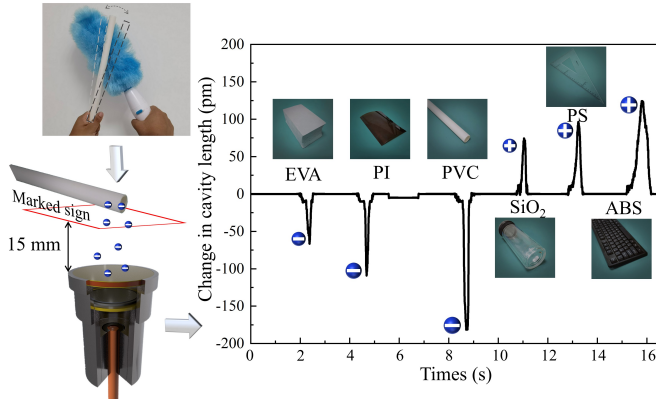


Fig. 5. Electrostatic response of the sensor to different samples

The six samples with different insulating dielectrics were rubbed by a brush, and the number of friction was 5. In addition, a red sign was marked to guarantee a fixed moving distance between the sensor and tested samples. The results indicated that the foam board made of ethylene-vinyl acetate copolymer (EVA), PI film and a plastic tube made of polyvinyl

chloride (PVC) carried the positive charges after the friction, while a glass made of SiO₂, a ruler made of polystyrene (PS), and a keyboard made of the acrylonitrile-butadiene-styrene copolymer (ABS) carried the negative charges after the friction. The results indicated that the sensor could not only capture the charges of the tested samples after friction, but also reflect the polarity of the tested samples.

3.2. Calibration of the sensor

The experimental setup was established to testify the performance of the sensor, as shown in Fig. 6[27]. The applied voltage of the electrode was 0~4.0 kV, which induced the changes of the cavity length. The incident light from the ASE was transmitted to the F-P cavity by ports 1 and 2 of 3 dB coupler. The reflected light in the F-P cavity via ports 2 and 3 was detected by the demodulator. The demodulator converted the light signal reflected from the sensor into the voltage signal, which was sent to the computer for signal processing.

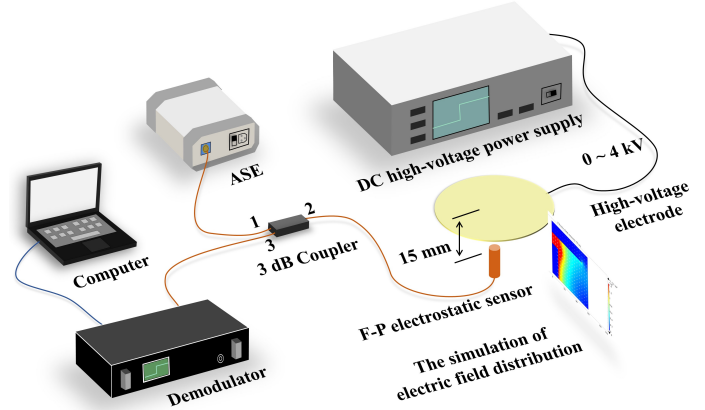


Fig. 6. Experimental setup of the F-P electrostatic sensor

The relationship between the change in the cavity length and the applied voltage is shown in Fig. 7(a). The output of the sensor had been recorded when the voltage varied from 0 to 4.0 kV in steps of 0.5 kV, and each experiment was repeated three times. The repeatability error (RE) of the sensor was 0.63%. Then, the electrostatic voltage from 1.0 to 4.0 kV was tested by the proposed sensor according to IEC 61000-4-2:2008[28]. As shown in Fig. 7(b), the sensor exhibits an excellent linearity of 0.99 and a sensitivity of 50.19 pm/kV. A nonlinear behavior is observed when the applied DC voltage is below 1.0 kV, which is induced by a high impedance of the electromechanical transducer[29]. The sensor still detects the electrostatic voltage under the nonlinear behavior, but at the cost of very low sensitivity.

Concerning to an improvement in sensitivity of the sensor, the performance of the electromechanical transducer could be improved by increasing the d_{33} according to Equation (3). Thus, the development and research of novel functional dielectrics with higher electromechanical conversion performance could contribute to the research of the electrostatic sensor[21,30]. For example, thermodynamic study of the electromechanical transducer can solve the problems in varying temperature environment for engineering applications.

As shown in Fig. 8(a), the thermal expansion of the electromechanical transducer was simulated, and the parameters of the electromechanical transducer were listed in

Table 1. The maximum surface displacement at 25 °C was employed as a benchmark to study the influence of temperature T on the displacement change ΔD . As shown in Fig. 8(b), the linear relationship between T and ΔD can provide the vital reference to the investigation of the temperature compensation technology of this sensor in the future. Then, the temperature compensation[31] based on the optical fiber sensing

multiplexing technique could be a promising pathway for the industrial and commercial application in the future. Additionally, the research on shielding materials and the miniaturization of the sensor will also be developed based on the MEMS technology. These approaches could be used to improve the performance of the electrostatic sensor.

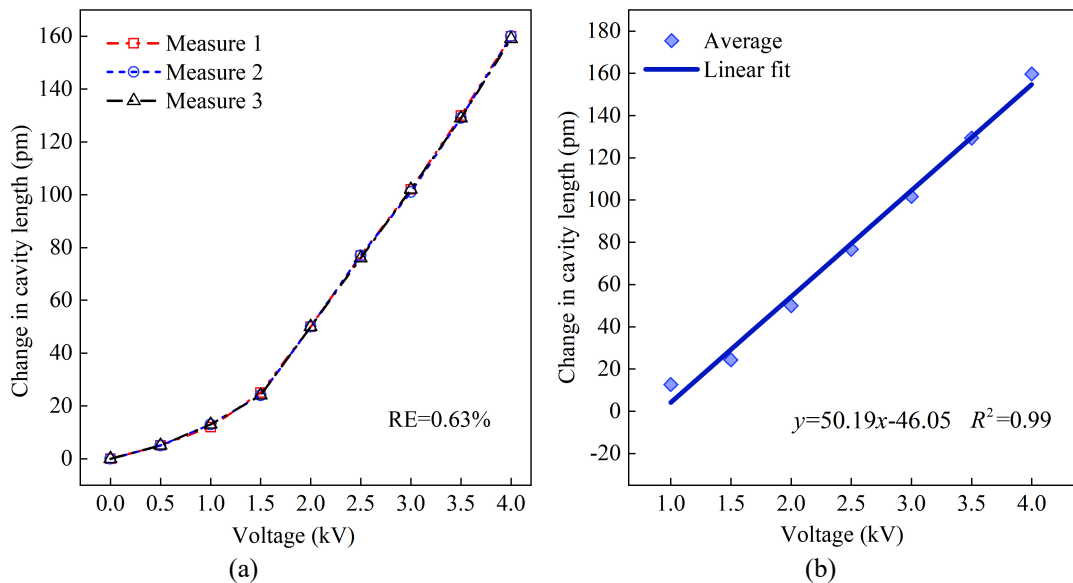


Fig. 7. Calibration results of the F-P electrostatic sensor
(a) Calibration curve of the sensor, (b) The linear response of sensor

Table 1 Material parameters of the electromechanical transducer

Materials	Coefficient of thermal expansion (1/K)	Thermal conductivity (W/(m·K))	Heat capacity at constant pressure (J/(kg·K))	Density (kg/m ³)	Young's modulus (Pa)	Poisson's ratio
Metal electrode (1 st)	1.95×10^{-5}	428	1.05×10^4	235	7.32×10^{11}	0.38
Piezoelectric ceramics	8×10^{-6}	1.45	420	7500	7.65×10^{10}	0.32
Metal electrode (2 nd)	2.03×10^{-5}	401	377	8440	9×10^{10}	0.324

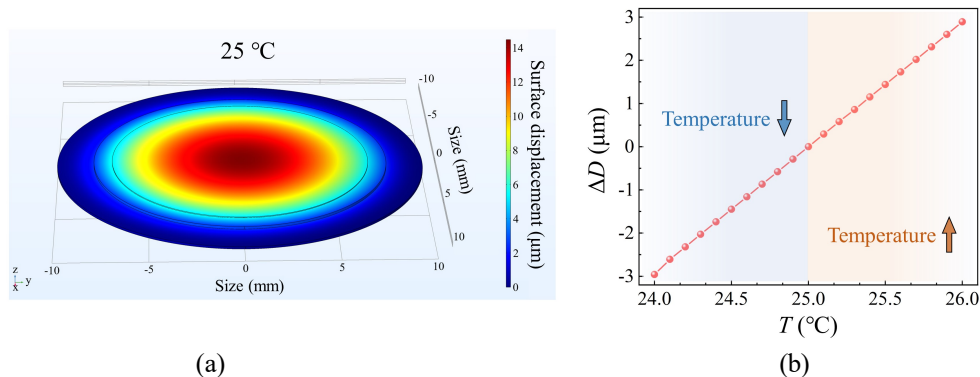


Fig. 8. Simulation of thermal expansion of the electromechanical transducer
(a) Surface displacement of the electromechanical transducer, (b) Simulation results of temperature change

4. Experiment

As an insulating polymer of electrical equipment, PI plays a significant role in stable operation and security of the electrical equipment. However, the accumulation of surface

charge leads to the changes of the surface morphology[32], which further influences the accumulation charge. As a result, some problems such as electrostatic discharge hazard and potential induced degradation are induced. To address these challenges, it is essential to explore the interactive influence

between the charge accumulation and surface morphology on PI.

The sample of PI with the dimension of 40 mm×40 mm×0.15 mm was rinsed by the anhydrous ethanol and employed to dry using a deionizing air blower. Fig. 9(a) shows the platform of the corona discharge, which consists of the needle-plate electrodes and DC high-voltage power supply. The experimental processes are as follows.

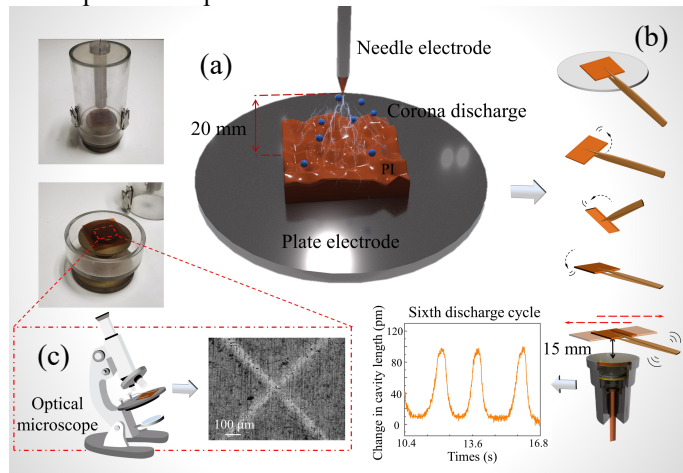


Fig. 9. Schematic diagram of the experimental process

- (a)The platform of the corona discharge,
 (b)Measurement process of the surface potential of PI,
 (c)Surface morphology of PI without discharge

Firstly, the surface morphology of the untreated PI was imaged by an optical microscope before the corona discharge and a “X” was marked as the center of the tested sample, as shown in Fig. 9. Secondly, PI was placed on the plate electrode where corona discharge was performed at 15.0 kV for 1 h. Thirdly, PI was clamped by the wooden tweezers to move back

and forth[25], as shown in Fig. 9(b). Then the surface potential of PI was measured by the sensor. Finally, the surface morphology at the marked “X” was observed by the optical microscope when the accumulated charge on PI completely dissipated. The experimental processes were repeated 15 times, and the relative humidity and temperature of the experiments were kept at 27%~35% and 25 °C, respectively.

5. Results and Discussion

As shown in Fig. 10(a), an increase tendency of the surface roughness of PI can be found when the discharge cycles increase. At the second discharge cycle, the surface morphology shows a few etched defects nearby the marked “X”, which is mainly induced by the ion mobility in the corona discharge process. Then, more defects are observed nearby the marked “X” at the fifth discharge cycle. Until the fourteenth discharge cycle, the etched defects can be observed on the entire discharged surface. The fact reveals an apparent etching effect from the ion mobility in the corona discharge process and its influence on the surface morphology of the sample.

The surface potential of PI measured by the F-P electrostatic sensor after discharge cycles is shown in Fig. 10(b). It can be concluded that the surface potential exhibits a negative quadratic trend[33] with the increase of the discharge cycles, which can be explained by the interactive influence between the charge accumulation and the surface morphology. According to Fig. 10(c), the surface of the untreated PI has a few defects. During the corona discharge, the peaks of the defects suffer from more discharge energy from the ion mobility, which accelerates the etching process of the initial peaks. The surface of PI tends to be smooth at the fifth discharge cycle, which enables that the discharge energy acts on the surface of PI evenly. Therefore, the charge accumulated on the surface of PI is increased. At the same time, the size of

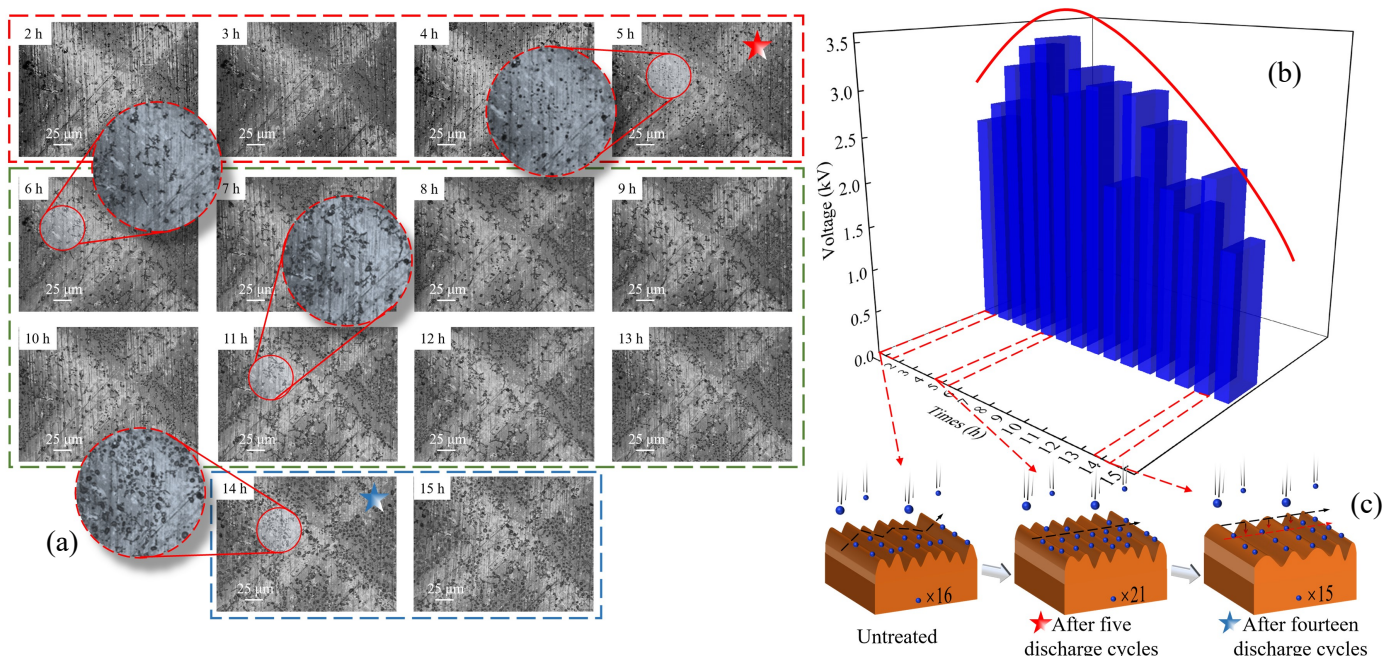


Fig. 10. Influence of surface morphology on the potential distribution of PI

- (a)Surface morphology of PI after the discharge cycles, (b)Surface potential distribution of PI under different discharge cycle,
 (c)Schematic diagram of the evolution of the surface morphology

the defects is enlarged during the fourteenth discharge cycle because the valley of the defect is etched. Therefore, the charge accumulated on the surface of PI is reduced. Thus, these experimental results can serve as an essential reference for relevant scholars in the fields of characterization of electrical insulation materials and triboelectric nanogenerator etc.

6. Conclusion

This paper presents a F-P electrostatic sensor based on the principle of F-P interference and electromechanical energy conversion. The sensor exhibits an excellent linearity of 0.99 and sensitivity of 50.19 pm/kV. The results show that the sensor has the merits of high linearity, passive monitoring, and anti-electromagnetic interference in the surface charge monitoring of insulating dielectrics. The results show that the optical sensor can not only identify the bipolar pattern of accumulated charge, but also reflect the influence of the surface roughness of the sample after discharge. Consequently, the passive F-P electrostatic sensor developed in this paper is expected to be widely applied in the fields of smart grid, fuel transportation, aerospace, IC industry, etc.

Acknowledgments

This work was supported by National Natural Science Foundation of China (No. 62061136009, 51877031). The author thanks the high-level talents plan of Shaanxi Province, the 'Belt and Road Initiative' Overseas Expertise Introduction Center for Smart Energy and Reliability of Transmission and Distribution Equipment of Shaanxi Province, the Youth Innovation Team of Shaanxi Universities for supporting this work. The authors would like to extend sincere gratitude to Ms. Feng Yan for her help in polishing English writing

Conflict of Interest

The authors declare no potential conflict of interests.

ORCID

Jia-Wei Zhang  <https://orcid.org/0000-0002-2947-0124>

REFERENCES

- [1] Li, C., et al.: The potentially neglected culprit of DC surface flashover: electron migration under temperature gradients. *Sci. Rep.* 7(1), 3271 (2017).
- [2] Qian, X., et al.: Quantitative characterization of pulverized coal and biomass-coal blends in pneumatic conveying pipelines using electrostatic sensor arrays and data fusion techniques. *Meas. Sci. Technol.* 23(8), 085307 (2012).
- [3] Wen, Z., Ma, X., Zuo, H.: Characteristics analysis and experiment verification of electrostatic sensor for aero-engine exhaust gas monitoring. *Measurement* 47, 633-644 (2014).
- [4] Chen, J., et al.: On-chip HBM and HMM ESD protection design for RF applications in 40 nm CMOS process. *IEEE Trans. Elect. Dev.* 65, 5267-5274 (2018).
- [5] Li, D., et al.: Charge accumulation characteristic on polymer insulator surface under AC voltage in air and C₄F₇N/CO₂ mixtures. *High Volt.* 5(2), 160-165 (2020).
- [6] Li, C., et al.: Insulator surface charge behaviors: from hazards to functionality. *IEEE Electr. Insul. Mag.* 38(3), 6-14 (2022).
- [7] Baytekin, H., et al.: Control of surface charges by radicals as a principle of antistatic polymers protecting electronic circuitry. *Science.* 341(6152), 1368-1371 (2013).
- [8] Murooka, Y., Takada, T., Hidaka, K.: Nanosecond surface discharge and charge density evaluation part I: review and experiments. *IEEE Electr. Insul. Mag.* 17(2), 6-16 (2001).
- [9] Davies, D.K.: The examination of the electrical properties of insulators by surface charge measurement. *J. Sci. Instrum.* 44(7), 521 (1967).
- [10] Du, B., et al.: Temperature-dependent surface charge and discharge behaviour of converter transformer oil-paper insulation under DC Voltage. *IET Sci. Meas. Technol.* 13(1), 29-34 (2019).
- [11] Zhang, B., et al.: Review of surface transient charge measurement on solid insulating materials via the Pockels technique. *High Volt.* 6(4), 608-624 (2021).
- [12] Liu, X., Kitamura, K., Terabe, K.: Surface potential imaging of nanoscale LiNbO₃ domains investigated by electrostatic force microscopy. *Appl. Phys. Lett.* 89(3), 132905 (2006).
- [13] Gégot, F., et al.: Experimental protocol and critical assessment of the Pockels method for the measurement of surface charging in a dielectric barrier discharge. *J. Phys. D: Appl. Phys.* 41(13), 135204 (2008).
- [14] Ma, G., et al.: Optical sensors for power transformer monitoring: A review. *High Volt.* 6(3), 367-386 (2021).
- [15] Zhang, J., et al.: An optical measurement method for nanosecond impulse signal monitoring of partial discharge based on the Fabry-Perot interferometer sensing system. *Jpn. J. Appl. Phys.* 61, 102006 (2022).
- [16] Zhang, Z., et al.: Oil-paper insulation partial discharge ultrasonic multifrequency sensing array based on fiber-optic Fabry-Perot sensor. *High Volt.* 7(2), 325-335 (2022).
- [17] Si W., et al.: Directional sensitivity of a MEMS-based fiber-optic extrinsic Fabry-Perot ultrasonic sensor for partial discharge detection. *Sensors* 18, 1975 (2018).
- [18] Chen W., et al.: Review of optical fibre sensors for electrical equipment characteristic state parameters detection. *High Volt.* 4(4), 271-281 (2019).
- [19] Zhang, J., et al.: Aging phenomena of backsheet materials of photovoltaic systems for future zero-carbon energy and the improvement pathway. *J. Mater. Sci. Technol.* 153, 106-119 (2023).
- [20] Zhang, J., et al.: Optical magnetic field sensors based on nanodielectrics: From biomedicine to IoT-based energy internet. *IET Nanodielectr.* 1-14 (2023).
- [21] Lim, Y., et al.: Modulating ZnO growth structures for maximum power output of hybrid piezo/triboelectric nanogenerator. *Adv. Funct. Mater.* (2022).
- [22] Liu, X., et al.: Study on energy and information storage properties of 2D-MXene/polyimide composites. *Compos. Part B Eng.* 241, 110014 (2022).
- [23] Lu, X., et al.: A miniature fiber-optic microphone based on annular corrugated MEMS diaphragm. *J. Lightw. Technol.* 36(22), 5224-5229 (2018).
- [24] Wen, Z., Hou, J., Atkin, J.: A review of electrostatic monitoring technology: the state of the art and future research

- directions. *Prog. Aerosp. Sci.* 94, 1-11 (2017).
- [25] Yan, Y., et al.: Electrostatic sensors-Their principles and applications. *Measurement* 169, 108506 (2021)
- [26] Zhang, J., et al.: Insulator condition monitoring based on F-P optical fiber leakage current sensor. *High Volt. Eng.* 48(8), 2915-2923 (2022).(in Chinese)
- [27] Zhang, K., Zhao, H., Zhang, Y.: A novel method to perform DC high-voltage measurements using an extrinsic Fabry-Perot interferometer. *J. Russ. Laser Res.* 36(5), 467-471 (2015).
- [28] Electromagnetic compatibility (EMC)-part 4-2: Testing and measurement techniques-electrostatic discharge immunity test. IEC 61000-4-2:2008.
- [29] Yañez, Y., et al.: Designing amplifiers with very low output noise for high impedance piezoelectric transducers. *NDT E Int.* 38(6), 491-496 (2005).
- [30] Liu, H., et al.: (K,Na)NbO₃-based lead-free piezoceramics: one more step to boost applications. *Natl. Sci. Rev.* 9, 101 (2022).
- [31] Liang, Z., et al.: FBG-based strain monitoring and temperature compensation for composite tank. *Aerosp. Sci. Technol.* 127, 107724 (2022).
- [32] Li, C., et al.: Charge cluster triggers unpredictable insulation surface flashover in pressurized SF₆. *J. Phys. D: Appl. Phys.* 54, 015308 (2021).
- [33] Yao, J., et al.: Investigation of granular surface roughness effect on electrostatic charge generation. *Adv. Powder Technol.* 28(9), 2003-2014 (2017)

How to cite this article: Author A, et al.: Article titles are set in sentence case, but capitalize proper nouns. *High Volt.* 00, 1-5 (2021). <https://doi.org/10.1049/hve.10001>